Journal of the Meteorological Society of Japan

EARLY ONLINE RELEASE

This is a PDF of a manuscript that has been peer-reviewed and accepted for publication. As the article has not yet been formatted, copy edited or proofread, the final published version may be different from the early online release.

This pre-publication manuscript may be downloaded, distributed and used under the provisions of the Creative Commons Attribution 4.0 International (CC BY 4.0) license. It may be cited using the DOI below.

The DOI for this manuscript is
DOI:10.2151/jmsj.2023-027
J-STAGE Advance published date: August 25th, 2023
The final manuscript after publication will replace the preliminary version at the above DOI once it is available.

Estimation of the equivalent depth of the Pekeris mode using reanalysis data

Hideaki Ishizaki

Graduate School of Science, Kyoto University, Kyoto, Japan

and

Takatoshi Sakazaki

Graduate School of Science, Kyoto University, Kyoto, Japan

and

Keiichi Ishioka

Graduate School of Science, Kyoto University, Kyoto, Japan

August 9, 2023

Corresponding author: Keiichi Ishioka, Graduate School of Science, Kyoto University, Kitashirakawa-Oiwake-cho, Sakyo-ku, Kyoto 606-8502, Japan.
E-mail: ishioka@gfd-dennou.org

Abstract

Inspired by two recent studies on the Pekeris mode, one of which first detected the Pekeris mode in satellite data after the eruption of the Hunga Tonga-Hunga Ha'apai (HTHH) volcano in January 2022, and the other of which obtained the theoretical equivalent depth of the Pekeris mode under the vertical temperature profile of the US Standard Atmosphere, the present manuscript calculates the theoretical equivalent depths of the Pekeris and Lamb modes under the realistic vertical temperature profile of the atmosphere after the eruption of the HTHH and longer period averages using global reanalysis data. The obtained equivalent depths depend to some extent on the location and range of the horizontal mean used to determine the vertical temperature profile, as well as the time and length of the temporal mean, but the equivalent depth of the Lamb mode is about 10.1 km, and that of the Pekeris mode is about 6.5 km. The reason why the equivalent depth of the Pekeris mode differs from the values obtained in the two recent studies mentioned above is also discussed.

1. Introduction

On 15 January, 2022, the Hunga Tonga-Hunga Ha'apai (HTHH) volcano erupted explosively, and the atmospheric waves generated by the eruption propagated globally. Watanabe, et al. (2022) detected two distinct wavefronts from the radiance observations of the Himawari-8 geostationary satellite. Based on comparison with the atmospheric general circulation model simulation results, it was concluded that the one with the faster phase velocity (315 m s^{-1}, corresponding to an equivalent depth of 10.1km) was the Lamb mode, while the slower one (245 m s^{-1}, corresponding to an equivalent depth of 6.1km) was the mode theoretically predicted by Pekeris (1937). The latter was called the Pekeris mode there, and this was the first detection of the Pekeris mode from observational data. Watanabe, et al. (2022) also showed that in the long-term spectral analysis of the ERA5 data, the power spectrum has peaks corresponding to the free oscillation modes of these two equivalent depths.

Inspired by Watanabe, et al. (2022), Ishioka (2023), based on the method proposed by Salby (1979) and correcting the problems of the method, calculated the equivalent depths of atmospheric free oscillations for the vertical temperature profile of the US Standard Atmosphere, 1976 (NOAA, et al., 1976), which we cite as USSA76, and obtained two values. One was 9.9 km for the Lamb mode and the other was 6.6 km for the Pekeris mode.

Comparing these values of the equivalent depths with those estimated by Watanabe, et al. (2022), the difference is 0.2 km for the Lamb mode and 0.5 km for the Pekeris mode, the difference being larger for the latter. Ishioka (2023) discussed that a possible reason for this difference is that USSA76 is a model of the mid-latitude atmosphere and the vertical temperature profile contained therein is different from that of the region where the Pekeris mode was excited and propagated after the eruption of the HTHH. In the present manuscript, we calculate the equivalent depths of the Lamb and Pekeris modes based on the method of Ishioka (2023) using vertical temperature profiles obtained by horizontally averaging global reanalysis data over various regions, including the equatorial region and the region around the HTHH at a time after the eruption or longer period averages, and examine how the difference in the vertical temperature profile affects the values of the theoretical equivalent depth of these two modes.

The remainder of the present manuscript is organized as follows. In Section 2, we describe the reanalysis data used and the horizontal/temporal averaging operations. The method of calculating the equivalent depths of the Lamb and Pekeris modes for the resulting vertical temperature profile is described in Section 3. The results of the calculation are presented in Section 4. Summary and discussion are given in Section 5.

2. Data and averaging methods

We use pressure-level (Hersbach, et al., 2023) and model-level (Hersbach, et al., 2017) temperature data in ERA5 (Hersbach, et al., 2020), the latest atmospheric reanalysis dataset produced by the European Centre for Medium-Range Weather Forecasts (ECMWF). The reason for using both pressure-level data and model-level data is that, as described in the next section, it is necessary to know the temperature profile up to near the mesopause when solving the vertical structure equation in order to accurately calculate the values of the equivalent depths of the free oscillation modes (Ishioka, 2023). Since the ERA5 pressure-level data are only available up to 1 hPa, the model-level data provided up to 0.01 hPa are used in conjunction with the pressure-level data. Specifically, the model-level data are used for the 54 levels from 0.01 hPa to 71.1187 hPa (each model level is defined in a hybrid coordinate, but down to that level it is completely identical to a pressure level), and the pressure-level data are used for the 27 levels from 100 hPa to 1000 hPa. The longitude-latitude grid interval we use is $1° \times 1°$ for the model-level data, while $0.25° \times 0.25°$ for the pressure-level data. For the time of data used, three types of data are used: hourly data at 08 UTC on 15 January 2022, approximately four hours after the HTHH eruption; data for the monthly average for January 2022; and data for the annual average for 2022. As mesospheric temperatures are known to be influenced by the 11-year solar activity cycle (Li, et al., 2021), the monthly average for January 2014, the most recent peak month, is also examined for comparison with January 2022, when solar activity was relatively moderate (for data on solar activity, see NOAA, 2023). Furthermore, an additional calculation is made for the 10-year average from January 2011 to December 2020 to check what the equivalent depths are in a climatological state.

To investigate the dependence of equivalent depths on the locations, the weighted average temperature $\overline{T}(p)$ is used with a horizontal averaging operation of the temperature field defined by the following equation.

$$\overline{T}(p) = \frac{\frac{1}{4\pi}\int_0^{2\pi}\int_{-\pi/2}^{\pi/2} F(\lambda,\phi)T(\lambda,\phi,p)\cos\phi \mathrm{d}\phi \mathrm{d}\lambda}{\frac{1}{4\pi}\int_0^{2\pi}\int_{-\pi/2}^{\pi/2} F(\lambda,\phi)\cos\phi \mathrm{d}\phi \mathrm{d}\lambda}. \tag{1}$$

Here, $T(\lambda,\phi,p)$ is the temperature at longitude λ, latitude ϕ, and pressure p, and $F(\lambda,\phi)$ is the horizontal weight function. The following six types of weight functions are used.

- global mean: $F(\lambda,\phi) = 1$
- tropical/extratropical average:

  - tropical average: $F(\lambda,\phi) = \begin{cases} 1 & (|\phi| \le 20^\circ), \\ 0 & (|\phi| > 20^\circ). \end{cases}$

  - extratropical average: $F(\lambda,\phi) = \begin{cases} 0 & (|\phi| \le 20^\circ), \\ 1 & (|\phi| > 20^\circ). \end{cases}$

- Averages taken in the vicinity/north/south of HTHH respectively

$$F(\lambda, \phi) = \exp(\alpha \cos c); \quad \cos c = \sin \phi_0 \sin \phi + \cos \phi_0 \cos \phi \cos(\lambda - \lambda_0) \tag{2}$$

  - Average taken in the vicinity of HTHH: $(\lambda_0, \phi_0) = (\lambda_T, \phi_T)$,
  - Average taken in the south of HTHH: $(\lambda_0, \phi_0) = (\lambda_T, \phi_T - 20°)$,
  - Averages taken in the north of HTHH: : $(\lambda_0, \phi_0) = (\lambda_T, \phi_T + 20°)$.

Here, $(\lambda_T, \phi_T) = (-175.39°, -20.55°)$ is the longitude and the latitude of HTHH (negative longitude represents west longitude and negative latitude represents south latitude), and c in (2) represents the angular distance along the great circle from the center point of longitude λ_0 and latitude ϕ_0. In (2), the function on the right-hand side gives a Gaussian-like weight function on the sphere. Here, $\alpha = 16$ is specified, which corresponds to a standard deviation of the Gaussian-like distribution with a spread of approximately 15° from the center point (Fig. 1). When the integrals in (1) are computed using the grid data, the integration in the longitude direction is performed by simply summing up the grid values and multiplying by the grid spacing in the longitude direction, while the Clenshaw-Curtis quadrature is used in the latitude direction. Figure 2 shows the vertical temperature profiles calculated by taking four different horizontal averages defined above: the global average, the tropical/extratropical average, and the average taken in the vicinity of HTHH, on the monthly mean data for January 2022. Fig. 1

The vertical temperature profile of USSA76 is also shown for reference. It can be seen that the temperature near the tropopause varies significantly depending on the type of horizontal averaging, whereas the stratospheric and mesospheric temperature profiles are less dependent on it. It should be noted here that the mesospheric temperatures are almost 10 K lower than USSA76. Figure 2 also shows the monthly average global mean vertical temperature profile for January 2014, as a period of peak solar activity; compared to the global mean for January 2022, the profiles almost overlap up to the stratopause, but above that, the temperature in January 2014 is higher and it is close to that of USSA76 near the mesopause. Fig. 2

3. Computation of equivalent depths

This section briefly describes a method for calculating the equivalent depths of free oscillation modes by numerically solving the vertical structure equation. The method is basically based on Ishioka (2023), where the geometric height is used as the vertical coordinate for consistency with Salby (1979), but here the logarithmic pressure coordinate is used as the vertical coordinate. This is because the ERA5 data are given in pressure coordinates. Since a fixed value of the scale height H has no meaning in the calculation of the equivalent depth itself, we set $H = 1$ (dimensionless) and define the logarithmic pressure coordinate $\hat{z} = -\ln(p/p_0)$, where p_0 is the surface pressure. With this setting, the vertical structure equations and the lower boundary conditions, Eqs. 25 and 26 of Ishioka (2023), can be expressed as follows.

$$\frac{\mathrm{d}^2 W}{\mathrm{d}\hat{z}^2} + \left(\frac{N_*^2}{g_0 h} - \frac{1}{4}\right) W = 0, \tag{3}$$

$$\frac{\mathrm{d}W}{\mathrm{d}\hat{z}} + \left(\frac{R\overline{T}}{g_0 h} - \frac{1}{2}\right) W = 0 \quad (\hat{z} = 0). \tag{4}$$

Here, g_0 is the gravity acceleration at the surface (set to 9.81 m s^{-2}) and R is the gas constant. In the present manuscript, unlike Ishioka (2023), we do not include the thermosphere in our calculations, thus R is assumed to be constant and we set $R = 287$ m^2 s^{-2} K^{-1}. The function W represents the vertical dependence of the amplitude of the disturbance in the log-pressure coordinate through the following equation: $\mathrm{d}\hat{z}/\mathrm{d}t \propto e^{\hat{z}/2}W$, where t is time. The squared log-pressure buoyancy frequency N_*^2 is written as,

$$N_*^2 = \frac{\mathrm{d}(R\overline{T})}{\mathrm{d}\hat{z}} + \kappa R\overline{T}. \tag{5}$$

Here, $\kappa = (\gamma - 1)/\gamma$ and γ is the specific heat ratio, which is set as $\gamma = 1.4$ in the present manuscript. That is, $\kappa = 2/7$.

The vertical structure equation (3) can be rewritten in the following simultaneous ordinary differential equations.

$$\frac{\mathrm{d}W}{\mathrm{d}\hat{z}} = V, \tag{6}$$

$$\frac{\mathrm{d}V}{\mathrm{d}z} + \left(\frac{N_*^2}{g_0 h} - \frac{1}{4}\right) W = 0. \tag{7}$$

Also, the lower boundary condition (4) can be expressed as,

$$V + \left(\frac{R\overline{T}}{g_0 h} - \frac{1}{2} \right) W = 0 \quad (\hat{z} = 0). \tag{8}$$

To impose the upper boundary condition, we also assume that $\overline{T}(\hat{z}) = T_{\rm t}(=$ const.) at $\hat{z} \geq \hat{z}_{\rm t}$, where $\hat{z}_{\rm t}$ is the uppermost $\hat{z}$ giving the vertical temperature profile. In this case, (3) becomes a differential equation with constant coefficients. If we introduce r as,

$$r = \frac{N_*^2}{g_0 h} - \frac{1}{4}, \tag{9}$$

then r is negative for the range of values of h corresponding to the equivalent depths of the Lamb and Pekeris modes, because in the present manuscript z_t is set near the mesopause where $\overline{T}$ is sufficiently low. The evanescent condition can be imposed as the upper boundary condition with this assumption of the vertical temperature profile as follows.

$$W(\hat{z}) \propto e^{-\sqrt{-r}\hat{z}} \quad (\hat{z} \geq \hat{z}_{\rm t}). \tag{10}$$

Since the vertical structure equation is a linear homogeneous equation and there remains an arbitrariness of constant multiples in the solutions, we can set as,

$$W = 1, \quad V = -\sqrt{-r} \quad (\hat{z} = \hat{z}_{\rm t}). \tag{11}$$

For a given h, we integrate the simultaneous ordinary differential equations (6) and (7) for (W, V) in the decreasing direction of $\hat{z}$ down to $\hat{z} = 0$ by using the classical 4th-order Runge-Kutta method with giving the starting point condition (11). Then we check the value of the left-hand side of the lower boundary condition (8) and search for h such that the left-hand side is zero. This determines the equivalent depths of the free oscillation modes. Here, the decrement used in the Runge-Kutta integration, $\Delta\hat{z}$ is set as $\Delta\hat{z} = \hat{z}_{\mathrm{t}}/10000$, which is smaller than 10 m when corresponding to the geometric height. The temperature, $\overline{T}$, at levels other than the pressure-level for which data are given in the reanalysis data is linearly interpolated in the coordinate system of $\hat{z}$. The vertical temperature gradient, $\mathrm{d}\overline{T}/\mathrm{d}\hat{z}$, which is needed to calculate the value of N_*^2, is also obtained as the slope of $\overline{T}(\hat{z})$ in the linearly interpolated interval.

The top boundary $\hat{z}_{\mathrm{t}}$ is basically set to the value of $\hat{z}$ corresponding to 0.01 hPa, the top model level of the ERA5 reanalysis data. However, according to Ishioka (2023), the value of the equivalent depth, especially for the Pekeris mode, can depend on the temperature near the mesopause. According to Xu, et al. (2007) and Smith (2012), the mesopause is 95-100 km high and its temperature is observed to be about 180 K, except in the region above the summer pole. Therefore, equivalent depth calculations are also performed for the case where temperature data ($\overline{T}_{\mathrm{t}}$ = 180 K or 170 K for a significantly lower case) are hypothetically given at the level of $p = 0.001$ hPa, as the top boundary.

The bottom boundary is also basically set to $p_0 = 1000$ hPa, which is the bottom of the pressure level for which the reanalysis data are given, but to check the dependence of the equivalent depth on the surface pressure difference, the same horizontal averaging operation as for the temperature data is performed on the sea level pressure data, and the equivalent depths are also calculated using the obtained value as p_0. In this case, if $p_0 > 1000$ hPa, the value of $\overline{T}$ there is determined by linear extrapolation.

4. Results

To illustrate the process of determining the equivalence depth, Fig. 3 shows how the left-hand side (denoted ϵ) of the lower boundary condition (8) varies with h. The temperature field data used here are the globally averaged monthly mean values for January 2022. The upper boundary is set to $p = 0.01$ hPa and the lower boundary to $p_0 = 1000$ hPa. From Fig. 3 it can be seen that at $h = 9.89$ km and $h = 6.43$ km the ϵ clearly crosses the zero line, giving equivalent depths there. The former corresponds to the equivalent depth of the Lamb mode and the latter to that of the Pekeris mode. The vertical structures of W corresponding to the solutions of these two equivalent depths are shown in Fig. 4. Here, $W \times e^{3\hat{z}/14}$ is drawn to facilitate comparison with Watanabe, et al. (2022)'s Fig. 8, rather than W itself. This should be constant for the Lamb mode if the atmosphere were

Fig. 3

isothermal. For the Lamb mode, the profile of W does not change sign, whereas for the Pekeris mode, a node is seen around $p \approx 270$ hPa. The p-coordinate of the position of this node is approximately 30 hPa larger p, *i.e.* at a lower altitude, than that calculated by Ishioka (2023) using USSA76 for the reference temperature profile. On the other hand, the GCM simulation results of Watanabe, et al. (2022) (Fig. 8b there) showed that the node in the Pekeris mode was located near 90 hPa, which is significantly at a higher altitude than the node position obtained in the present manuscript. Fig. 4

In the same way as illustrated in Fig. 3, the equivalent depths of the Lamb and Pekeris modes are calculated and tabulated in Table 1 for the vertical temperature profiles obtained by the various area and time averaging methods described in Section 2. Also included are the equivalent depth values when the upper boundary is set to 0.001 hPa and two kinds of temperatures are imposed there and when p_0 is taken as the mean sea level pressure, as described in Section 3.

As shown in Table 1, the equivalent depths of the Lamb modes do not strongly depend on the method of temporal or horizontal averaging of the data, and are within the range of 9.9 km to 10.1 km when rounded to one decimal place, except for the extratropical average. When the global average is used, the obtained equivalent depth value is 9.9 km in rounded to one decimal place. This value is consistent with the value obtained by Ishioka

(2023) where USSA76 temperature profile was used. This agreement can be attributed to the temperature profile in the lower troposphere being close to that of the USSA76, as shown in Fig. 2. However, the values are slightly larger in the region around HTHH, in the north of HTHH, and in the tropics, which reflects the higher tropospheric temperatures in these regions. The equivalent depths close to 10.1 km for these regions are consistent with the estimate of the equivalent depth of the Lamb mode by Watanabe, et al. (2022).

The equivalent depth of the Pekeris mode shown in Table 1 is 6.4 km or 6.5 km to two significant digits, which does not strongly depend on the method of temporal or horizontal averaging of the data except for the extratropical average and the global average with the 170 K mesopause temperature case (column F). Again, the equivalent depth of the Pekeris mode is larger in the region around the HTHH, in the north of the HTHH, and in the tropics, reflecting the higher tropospheric temperatures in these regions. Both of the values, 6.4 km and 6.5 km, are smaller than the value of 6.6km obtained by Ishioka (2023). This discrepancy can be attributed to the lower temperature near and above the stratopause for the reanalysis data than that for USSA76, as shown in Fig. 2. Although the equivalent depth of the Lamb mode obtained in the present manuscript is in agreement with the estimate in Watanabe, et al. (2022), that of the Pekeris mode obtained in the present manuscript is close to 6.5 km in the region around the HTHH, in the north of the HTHH, and in the tropics, except for the cases with the low mesopause temperature settings (columns E and F), which differs from the estimate of 6.1 km in Watanabe, et al. (2022). Furthermore, Watanabe, et al. (2022) showed that the wavefronts considered to be the Pekeris mode propagated from the HTHH at a speed of about 245 ms^{-1} to the north and about 270 ms^{-1} to the south, and if this estimated phase speed is directly converted into the equivalent depth, it is expected that the equivalent depth in the south of the HTHH is larger than that in the north of the HTHH. However, the calculation results in Table 1 show the opposite, which is also inconsistent with the results of Watanabe, et al. (2022).

Before closing this section, the dependence of the equivalent depth of the Lamb mode and Pekeris mode on the setting of p_0, where the lower boundary condition is imposed, and the temperature setting given at the mesopause, described at the end of Section 3, is examined. Comparing columns A and D of Table 1, we can see the difference between the case where the value of p_0 is 1000 hPa (column A) and the case where it is the horizontal mean of the sea level pressure (column D) for the monthly mean data in January 2022: for both the Lamb and Pekeris modes, the equivalent depth changes by only about 0.01 km. Therefore, small differences in the value of p_0 are insignificant. A similar insignificance holds when considering the effects of water vapor. Although not shown in the table, when equivalent depths are calculated using virtual temperatures, which can be calculated from specific humidity data, instead of temperatures, the equivalent depth for the Lamb mode is only 0.02 km larger at most in the tropical mean, where the effect is most significant. Furthermore, the Pekeris mode only increases by about 0.002 km at most, so the effect of water vapor can be ignored when discussing to one decimal place.

To check the dependence of the equivalent depth values on the temperature setting at the mesopause, we should compare columns E and F with column A of Table 1. For the Lamb mode, the equivalent depth does not change to the second decimal place as the temperature setting is changed at the mesopause. This reflects the fact that the Lamb mode has much lower energy density in the mesosphere than in the troposphere and stratosphere (Salby, 1979, Fig. 4c). On the other hand, for the Pekeris mode, the values in columns E and F are smaller than that in column A and, in particular, when a significantly low temperature of 170 K is assumed (column F) at $p = 0.001$ hPa, the first decimal place can change. This difference with the Lamb mode with regard to the dependence on temperature setting at mesopause is understood to be due to the fact that the Pekeris mode has an energy density of some magnitude even in the mesosphere (Salby, 1979, Fig. 5c). However, even with such extreme mesopause temperature settings, the equivalent depth of the vertical temperature profile averaged around the HTHH is only reduced to about 6.4 km, which does not fill the gap with the estimation of the equivalent depth of the Pekeris mode in Watanabe, et al. (2022), 6.1 km.

Table 1

At the end of this section, let us examine the effects of solar activity. We compare columns G with column A of Table 1. The equivalent depth of the Lamb mode is only about 0.02 km larger in January 2014, when solar activity was at its peak, than in January 2022, but the equivalent depth of the Pekeris mode is about 0.2 km larger, reflecting that the Pekeris mode is strongly influenced by the higher mesospheric temperatures during the peak period of solar activity. However, if we take the 10-year average from 2011 to 2020 (column H) and compare it with the annual average for 2022 (column C), the difference in equivalent depth values between the two is at most 0.01 km for the Lamb mode and 0.03 km for the Pekeris mode, that is, the annual average for 2022 is close to the 10-year average from 2011 to 2020. For both columns C and H, the equivalent depth of the Lamb mode, rounded to the first decimal place, is 10.1 km and that of the Pekeris mode equivalent depth is 6.5 km in the tropics.

5. Summary and discussion

In the present manuscript, inspired by the detection of the Pekeris mode after the HTHH eruption by Watanabe, et al. (2022), and following the method of Ishioka (2023), we calculated the theoretical equivalent depths of the Lamb and Pekeris modes for the vertical temperature profiles obtained by horizontally averaging reanalysis data. For the horizontal averaging, six different horizontal averages were examined: the global average, the tropical/extratropical average, and the average taken in the vicinity/north/south of HTHH. For the time direction, the following three types of data were analyzed: hourly data at 08 UTC on 15 January 2022, approximately four hours after the HTHH eruption; data for the monthly average for January 2022; and data for the annual average for 2022. The equivalent depth values for the Lamb and Pekeris modes were found to depend on the horizontal averaging method, but not so much on the temporal averaging method. The obtained value of the equivalent depth of the Lamb mode is in the range of 9.9 km to 10.1 km when rounded to one decimal place, except for the extratropical average. That of the Pekeris mode is 6.4 km or 6.5 km except for the cases with the low mesopause temperature settings. For comparison with the estimate in Watanabe, et al. (2022), if we restrict the discussion to the cases where the horizontal average is taken in the vicinity/north of HTHH and in the tropics, the obtained equivalent depths for the Lamb and the Pekeris modes were 10.1 km and 6.5 km, respectively, when rounded to one decimal place. This equivalent depth of the Lamb mode is in good agreement with the estimate in Watanabe, et al. (2022), but that of the Pekeris mode is significantly larger than the value of 6.1km estimated by Watanabe, et al. (2022). The calculated equivalent depth of the Pekeris mode can be as small as 6.4 km if significant low temperatures are hypothetically imposed at the mesopause, but it is still clearly larger than the value of 6.1 km estimated in Watanabe, et al. (2022).

Although the estimation of the equivalent depth of the Pekeris mode is based on the classical tidal theory where the effect of mean winds is ignored and the Pekeris mode could be sensitive to the very strong mean winds in both the tropical and extratropical middle atmosphere, we suspect that in the detection of Pekeris modes in Watanabe, et al. (2022) captured transient states rather than fully modal states, leading to the discrepancy. One basis for our suspicion is Fig. 9d of Watanabe, et al. (2022), where they performed a spectral analysis of 57 years of hourly global reanalysis data and the equivalent depth of the Pekeris mode was set to 6.1 km and the correspondence with the spectral peak was examined. Figure 5 shows the same figure as Fig. 9d of Watanabe, et al. (2022), except with the additional line of the peak when the equivalent depth of the Pekeris mode is set to 6.5 km. It is clear that the additional line with the equivalent depth of 6.5 km is more consistent with the spectral peak, and the value obtained in the present manuscript is considered to be more consistent, at least climatologically, with the equivalent depth of the Pekeris mode. Another basis for our suspicion is the difference in the position of the nodes in the Pekeris mode as described in the previous section. The GCM simulation for the period of the satellite data-based detection of the Pekeris mode in Watanabe, et al. (2022) showed that the node of the p-velocity corresponding to the Pekeris mode was located near 90 hPa, which is significantly at a higher altitude than the node position obtained in the present manuscript. We speculate that the difference in the position of the nodes is due to the mixing of internal gravity wave modes other than the Pekeris modes at the time when the Pekeris mode is detected in Watanabe, et al. (2022), resulting in the slower wavefront phase velocity compared to the theoretical estimate in the present manuscript. In order to test the validity of this speculation, it is necessary to simulate the excitation of waves by the eruption and to separate the Pekeris modes from other gravity modes by a global numerical model calculation that includes a sufficiently high altitude region and imposes appropriate radiative boundary conditions to avoid the influence of reflected waves at the boundary. Performing such numerical experiments to clarify how the Pekris mode is generated by the eruption will be our future task and the effects of the mean flow mentioned above should also

Fig. 5

be examined there.

Data Availability Statement

For the ERA5, pressure-level data (Hersbach, et al., 2023) were downloaded from https://cds.climate.copernicus.eu/cdsapp#!/dataset/reanalysis-era5-pressure-levels?tab=overview, while model-level data (Hersbach et al., 2017) were obtained through the Meteorological Archival and Retrieval System (MARS).

Acknowledgments

We thank two anonymous reviewers for their helpful comments. This work was supported by JSPS KAKENHI Grant Numbers 20K04061. Python and many other libraries including matplotlib were used to draw figures.

References

Hersbach, H., and Coauthors, 2017: Complete ERA5 from 1950: Fifth generation of ECMWF atmospheric reanalyses of the global climate. Copernicus Climate Change Service (C3S) Data Store (CDS). (Last Accessed on 31-Mar.-2023)

Hersbach, H., and Coauthors, 2020: The ERA5 global reanalysis. Quart. J. Roy. Meteor. Soc., 146, 1999–2049, https://doi.org/10.1002/qj.3803

Hersbach, H., and Coauthors, 2023: ERA5 hourly data on pressure levels from 1940 to present. Copernicus Climate Change Service (C3S) Climate Data Store (CDS), DOI: 10.24381/cds.bd0915c6 (Last Accessed on 7-Nov.-2022): ERA5 monthly averaged data on pressure levels from 1940 to present. Copernicus Climate Change Service (C3S) Climate Data Store (CDS), DOI: 10.24381/cds.6860a573 (Last Accessed on 1-Apr.-2023): ERA5 monthly averaged data on single levels from 1940 to present. Copernicus Climate Change Service (C3S) Climate Data Store (CDS), DOI: 10.24381/cds.f17050d7 (Last Accessed on 22-Mar.-2023):

Ishioka, K., 2023: What is the equivalent depth of the Pekeris mode? *Journal of the Meteorological Society of Japan*, **101**, 139–148.

Li, T., J. Yue, J. M. Russell III, and X. Zhang, 2021: Long-term trend and solar cycle in the middle atmosphere temperature revealed from merged HALOE and SABER datasets. *Journal of Atmospheric and Solar-Terrestrial Physics*, **212**, 105506.

NOAA, 2023: SOLAR CYCLE PROGRESSION, https://www.swpc.noaa.gov/products/solar-cycle-progression (Accessed on Aug. 1/2023).

NOAA, NASA, and USAF, 1976: *U.S. STANDARD ATMOSPHERE, 1976*. U.S. Government Printing Office, 227pp.

Pekeris, C. L., 1937: Atmospheric oscillations. *Proceedings of the Royal Society of London*, **A158**, 650–671.

Salby, M. L., 1979: On the solution of the homogeneous vertical structure problem for long-period oscillations. *Journal of the Atmospheric Sciences*, **36**, 2350–2359.

Smith, A. K., 2012: Global Dynamics of the MLT. *Surveys in Geophysics* **33**, 1177–1230.

Watanabe, S., K. Hamilton, T. Sakazaki, and M. Nakano, 2022: First Detection of the Pekeris Internal Global Atmospheric Resonance: Evidence from the 2022 Tonga Eruption and from Global Reanalysis Data. *Journal of the Atmospheric Sciences*, **79**, 3027–3043.

Xu, J., H. L. Liu, W. Yuan, A. K. Smith, R. G. Roble, C. J. Mertens, J. M. Russell III, and M. G. Mlynczak, 2007: Mesopause structure from thermosphere, ionosphere, mesosphere, energetics, and dynamics (TIMED)/sounding of the atmosphere using broadband emission radiometry (SABER) observations. *Journal of Geophysical Research: Atmospheres*, **112**, D09102.

List of Figures

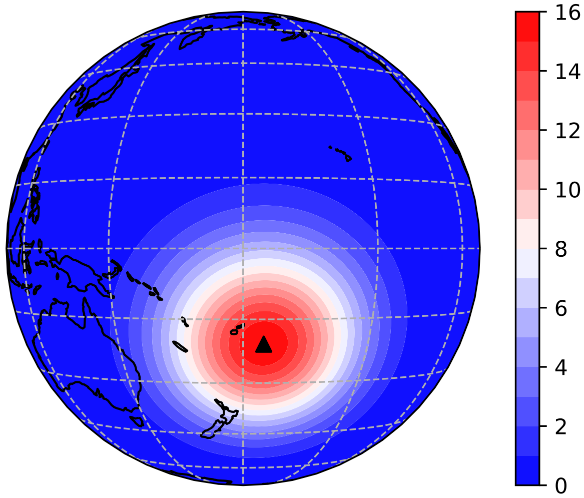

Fig. 1. Distribution of the weight function $F(\lambda, \phi)$ with setting $(\lambda_0, \phi_0) = (\lambda_T, \phi_T)$ in (2). The triangular symbol indicates the location of Hunga Tonga-Hunga Ha'apai volcano.

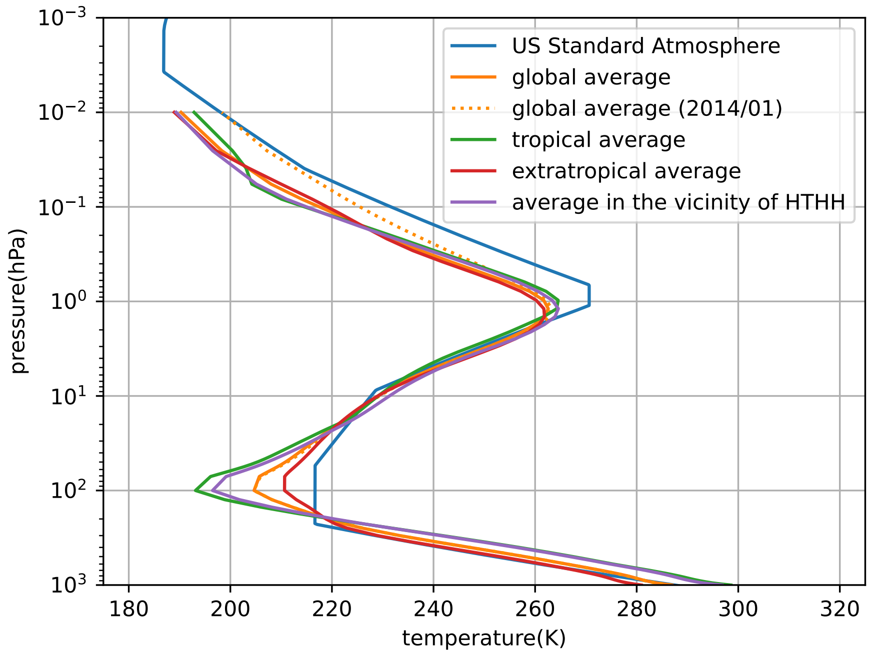

Fig. 2. Vertical temperature profiles obtained by taking various horizontal averages of the January 2022 monthly average of ERA5 data. Explanations on the correspondence between the color of the curves and the type of average are written in the figure. Note that the orange dotted curve shows the January 2014 monthly average.

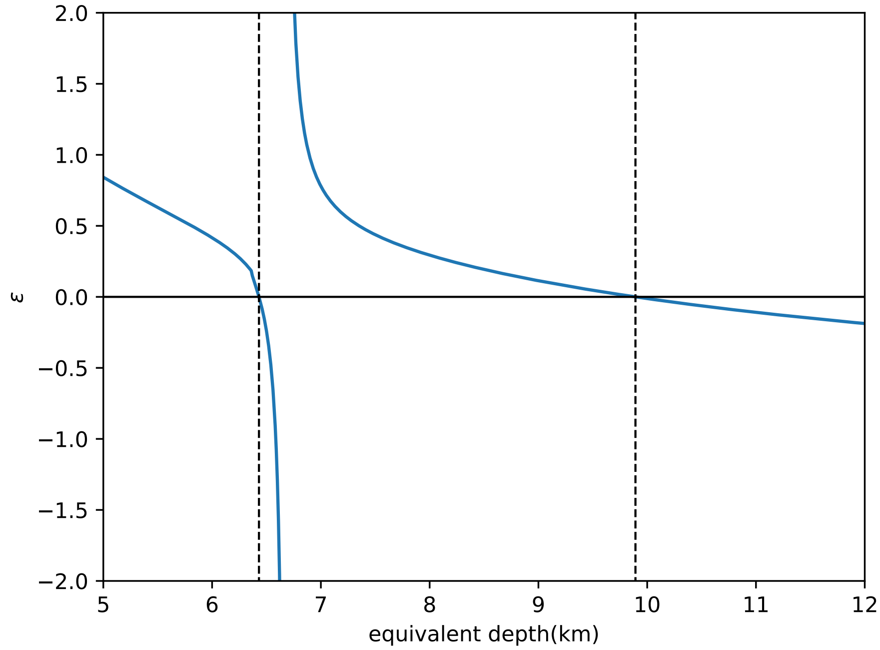

Fig. 3. Dependence of the error ϵ of the lower boundary condition on the equivalent depth h given a globally averaged vertical profile of monthly mean temperature for January 2022.

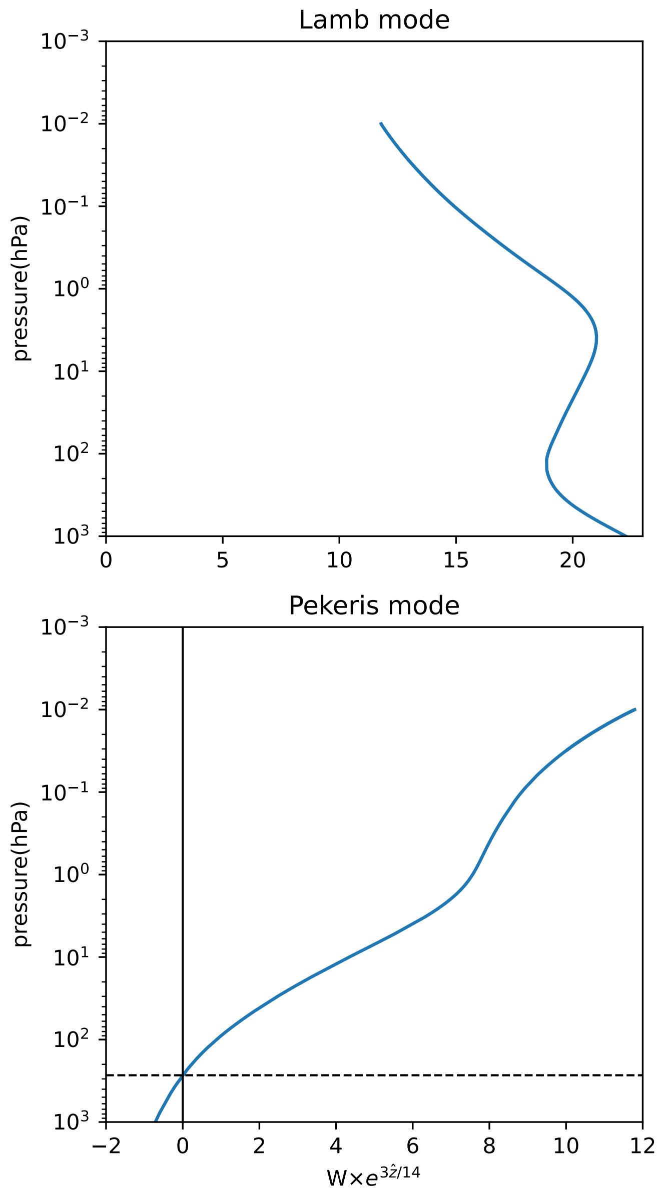

Fig. 4. Vertical profiles of $W \times e^{3\hat{z}/14}$ for two equivalent depth solutions given a globally averaged vertical profile of monthly mean temperature for January 2022. (Upper figure: Lamb mode ($h = 9.89$ km), lower figure: Pekeris mode ($h = 6.43$ km)).

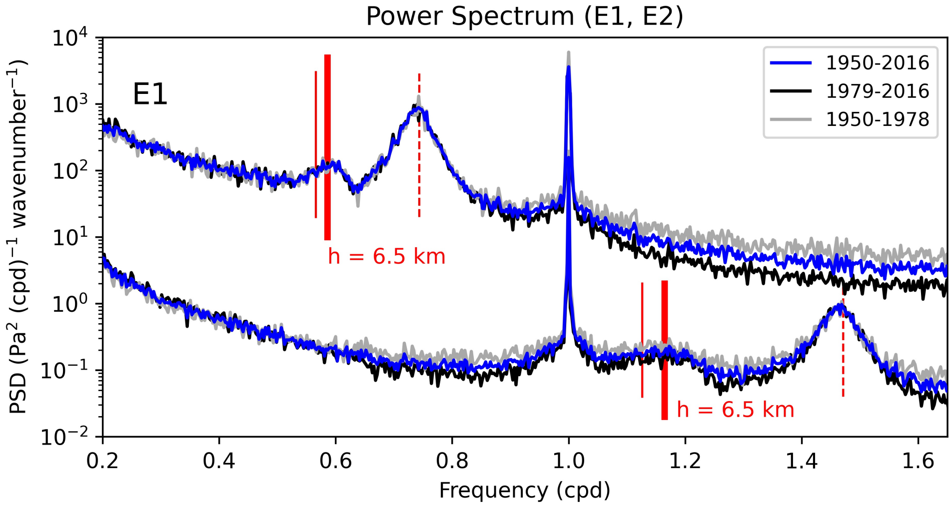

Fig. 5. Zonal wavenumber-frequency spectrum for equatorially symmetric surface pressure (during 1950–2016) averaged for 20°S–20°N, as adopted by Fig. 9d of Watanabe et al. (2022) with a slight modification. Thin, red dashed and solid vertical lines indicate the theoretically predicted resonant frequencies for h = 10.1 km and 6.1 km, respectively, while thick, red vertical lines are for those for h = 6.5 km. ©American Meteorological Society. Used with permission.

List of Tables

Table 1. The calculated equivalent depths for the Lamb and the Pekeris mode (km). Columns A–H are as follows. A: the monthly mean for January 2022, B: the hourly mean at 08 UTC on 15 January 2022, C: the annual mean for 2022, D: the monthly mean for January 2022 with surface pressure as sea level pressure, E: the monthly mean for January 2022 with $\overline{T} = 180$ K at the level of $p = 0.001$ hPa, F: the monthly mean for January 2022 with $\overline{T} = 170$ K at the level of $p = 0.001$ hPa, G: the monthly mean for January 2014, H: the 10-year average from January 2011 to December 2020.

	A	B	C	D	E	F	G	H
Lamb mode								
global average	9.89	9.89	9.91	9.90	9.89	9.89	9.90	9.91
tropical average	10.06	10.06	10.08	10.07	10.06	10.06	10.06	10.09
extratropical average	9.81	9.81	9.82	9.82	9.81	9.81	9.83	9.82
vicinity of HTHH	10.07	10.08	10.02	10.08	10.07	10.07	10.07	10.02
north of HTHH	10.07	10.08	10.07	10.08	10.07	10.07	10.07	10.08
south of HTHH	10.01	10.01	9.86	10.02	10.01	10.01	10.02	9.87
Pekeris mode								
global average	6.43	6.44	6.46	6.43	6.36	6.33	6.64	6.47
tropical average	6.52	6.53	6.48	6.52	6.43	6.40	6.75	6.51
extratropical average	6.39	6.39	6.45	6.39	6.32	6.29	6.58	6.45
vicinity of HTHH	6.47	6.46	6.47	6.47	6.42	6.39	6.69	6.48
north of HTHH	6.50	6.50	6.47	6.51	6.43	6.40	6.74	6.51
south of HTHH	6.40	6.41	6.46	6.41	6.39	6.36	6.56	6.45